[^{18}F]Fluoromethyl-[1,2-$^{2}H_4$]-Choline: A Novel Radiotracer for Imaging Choline Metabolism in Tumors by Positron Emission Tomography

Julius Leyton,[1] Graham Smith,[1] Yongjun Zhao,[2] Meg Perumal,[1] Quang-De Nguyen,[1] Edward Robins,[2] Erik Årstad,[2] and Eric O. Aboagye[1]

[1]Molecular Therapy Group, Faculty of Medicine, Imperial College London; [2]MDx Discovery (part of GE Healthcare) at Hammersmith Imanet Ltd., Hammersmith Hospital, London, United Kingdom

Abstract

Current radiotracers for positron emission tomography imaging of choline metabolism have poor systemic metabolic stability *in vivo*. We describe a novel radiotracer, [^{18}F]fluoromethyl-[1,2-$^{2}H_4$]-choline (D4-FCH), that employs deuterium isotope effect to improve metabolic stability. D4-FCH proved more resistant to oxidation than its nondeuterated analogue, [^{18}F]fluoromethylcholine, in plasma, kidneys, liver, and tumor, while retaining phosphorylation potential. Tumor radiotracer levels, a determinant of sensitivity in imaging studies, were improved by deuterium substitution; tumor uptake values expressed as percent injected dose per voxel at 60 min were 7.43 ± 0.47 and 5.50 ± 0.49 for D4-FCH and [^{18}F]fluoromethylcholine, respectively (P = 0.04). D4-FCH was also found to be a useful response biomarker. Treatment with the mitogenic extracellular kinase inhibitor PD0325901 resulted in a reduction in tumor radiotracer uptake that occurred in parallel with reductions in choline kinase A expression. In conclusion, D4-FCH is a very promising metabolically stable radiotracer for imaging choline metabolism in tumors. [Cancer Res 2009;69(19):7721–8]

Introduction

The biosynthetic product of choline kinase (EC 2.7.1.32) activity, phosphocholine, is elevated in several cancers and is a precursor for membrane phosphatidylcholine (1–4). Overexpression of choline kinase and increased enzyme activity have been reported in prostate, breast, lung, ovarian, and colon cancers (5–10) and are largely responsible for the increased phosphocholine levels with malignant transformation and progression; the increased phosphocholine levels in cancer cells are also due to increased breakdown via phospholipase C (6). Because of this phenotype, together with reduced urinary excretion, [^{11}C]choline has become a prominent radiotracer for positron emission tomography (PET) and PET-computed tomography imaging of prostate cancer and, to a lesser extent, imaging of brain, esophageal, and lung cancers (11–16). The specific PET signal is due to transport and phosphorylation of the radiotracer to [^{11}C]phosphocholine by choline kinase. [^{18}F]Fluoromethylcholine (FCH) was developed to overcome the short physical half-life of carbon-11 (20.4 min; ref. 17) and several PET and PET-computed tomography studies with this relatively new radiotracer have been published (18–21). The longer half-life of fluorine-18 (109.8 min) was deemed potentially advantageous in permitting late imaging of tumors when sufficient clearance of parent tracer in systemic circulation had occurred (22). Of interest, however, [^{11}C]choline (and fluoro-analogue) is oxidized to [^{11}C]betaine by choline oxidase (EC 1.1.3.17) mainly in kidney and liver tissues, with metabolites detectable in plasma soon after injection of the radiotracer (23). This makes discrimination of the relative contributions of parent radiotracer and catabolites difficult when a late imaging protocol is used. In this article, we have developed a more metabolically stable FCH analogue, [^{18}F]fluoromethyl-[1,2-$^{2}H_4$]-choline (D4-FCH), based on the deuterium isotope effect (24–27). This novel radiotracer has several potential advantages: (*a*) due to improved stability, it should better enable late imaging of tumors after sufficient clearance of the radiotracer from systemic circulation and (*b*) it should enhance the sensitivity of tumor imaging through increased availability of substrate. In this article, we report for the first time the development of D4-FCH for imaging tumors and for monitoring therapeutic response.

Materials and Methods

Radiopharmaceuticals and drug. No-carrier-added FCH and D4-FCH were synthesized by reacting [^{18}F]fluorobromomethane with *N, N*-dimethylaminoethanol or D4-*N, N*-dimethylaminoethanol, respectively, as shown in Fig. 1*A*. [^{18}F]Fluorobromomethane was synthesized from dibromomethane by substitution of bromine with [^{18}F]fluoride based on the method reported by Bergman and colleagues (28). After trapping the [^{18}F]fluorobromomethane into a 2.5 mL conical glass vial containing 150 μL dimethylaminoethanol or D4-*N, N*-dimethylaminoethanol in dry acetonitrile (1.0 mL) precooled to 0°C, the vial was sealed and heated to 100°C for 10 min. The solvent was removed by a stream of nitrogen. Following this, the residue containing FCH or D4-FCH was dissolved in 5% ethanol solution (10 mL) and loaded onto a cation exchange Sep-Pak Cartridge (Waters, Accell CM light), which had been preconditioned with 2 mol/L HCl and water (5 mL each). After further washing of the CM cartridge with ethanol and water (10 mL each), the FCH or D4-FCH was eluted with sterile isotonic saline (0.5-2.0 mL) and sterilized by filtration (0.22 μm sterile filter; Millipore, Waters).

The radiochemical purity for both FCH and D4-FCH was ~99% as analyzed with radiochemical detection [radio–high-performance liquid chromatography (HPLC)]. The radioactive species were confirmed as the desired choline analogues by coelution with a commercial fluorocholine chloride standard (obtained from ABCR) by HPLC on an Agilent 1100 series HPLC system equipped with a Bioscan Flowcount FC-3400 Pin diode detector (for radioactivity detection) and an Agilent G1362A refractive index detector for detection of nonradioactive species. The stationary phase comprised a Phenomenex Luna C_{18} reverse-phase column (150 × 4.6 mm) and the mobile phase comprised 5 mmol/L heptanesulfonic acid (pH 8.0) and acetonitrile (90:10 v/v) delivered at a flow rate 1 mL/min. [^{11}C]Choline was synthesized by Hammersmith Imanet using a previously described

Note: Supplementary data for this article are available at Cancer Research Online (http://cancerres.aacrjournals.org/).

Requests for reprints: Eric O. Aboagye, Molecular Therapy Group, Faculty of Medicine, Imperial College London, Room 240, MRC Cyclotron Building, Hammersmith Hospital, Du Cane Road, London W12 ONN, United Kingdom. Phone: 44-2083833759; Fax: 44-2083831783; E-mail: eric.aboagye@imperial.ac.uk.

©2009 American Association for Cancer Research.

doi:10.1158/0008-5472.CAN-09-1419

Downloaded from http://aacrjournals.org/cancerres/article-pdf/69/19/7721/2614729/7721.pdf by guest on 21 February 2024

method (29). PD0325901 (*N*-[(*R*)-2,3-dihydroxy-propoxy]-3,4-difluoro-2-(2-fluoro-4-iodo-phenylamino)-benzamide) was obtained from the Division of Signal Transduction Therapy, University of Dundee.

Animals and tumor models. All animal experiments were done by licensed investigators in accordance with the United Kingdom Home Office Guidance on the Operation of the Animal (Scientific Procedures) Act 1986 and within guidelines set out by the United Kingdom Coordinating Committee for Cancer Research's Ad hoc Committee on Welfare of Animals in Experimental Neoplasia (30). Both tumor-bearing (BALB/c nude mice) and non-tumor-bearing (BALB/c mice) animals were used. Human melanoma, SKMEL-28, and human colon, HCT116, tumors were grown in BALB/c *nu/nu* mice (Harlan) as reported previously (31). Tumor dimensions were measured continuously using a caliper and tumor volumes were calculated by the equation: volume = $(\pi / 6) \times a \times b \times c$, where *a*, *b*, and *c* represent three orthogonal axes of the tumor. Mice were used when their tumors reached ~ 100 mm^3.

Oxidation potential of FCH and D4-FCH *in vivo*. FCH or D4-FCH (~ 4.8 MBq) was injected via the tail vein into anesthetized non-tumor-bearing BALB/c mice or HCT116 tumor-bearing BALB/c nude mice; isofluorane/O_2/N_2O anesthesia was used. In a limited number of cases, [^{11}C]choline (~ 9 MBq) was used for comparison. Plasma samples were obtained at 2, 15, 30, and 60 min after injection; liver, kidney, and tumor samples were obtained at 30 min. All samples were snap-frozen in liquid nitrogen. For analysis, samples were thawed and kept at 4°C immediately before use. To ~ 0.2 mL plasma was added ice-cold methanol (1.5 mL). The mixture was then centrifuged (3 min, 15,493 × *g*, 4°C). The supernatant was evaporated to dryness using a rotary evaporator (Heidoloph Instruments) at a bath temperature of 40°C. The residue was suspended in mobile phase (1.1 mL), clarified (0.2 μm filter), and analyzed by HPLC. Liver, kidney, and tumor samples were homogenized in ice-cold methanol (1.5 mL) using an IKA Ultra-Turrax T-25 homogenizer and subsequently treated as per plasma samples. All samples were analyzed by radio-HPLC on an Agilent 1100 series HPLC system (Agilent Technologies) equipped with a γ-RAM Model 3 γ-detector (IN/US Systems) and Laura 3 software (Lablogic). The stationary phase comprised a Waters μBondapak C_{18} reverse-phase column (300 × 7.8 mm). Samples were analyzed using a mobile phase comprising solvent A (acetonitrile/water/ethanol/acetic acid/1.0 mol/L ammonium acetate/0.1 mol/L sodium phosphate; 800/127/68/2/3/10) and solvent B (acetonitrile/water/ethanol/acetic acid/1.0 mol/L ammonium acetate/0.1 mol/L sodium phosphate; 400/400/68/44/88/10) with a gradient of 0% B for 6 min, then 0 → 100% B in 10 min, 100% B for 0.5 min, 100 → 0% B in 1.5 min then 0% B for 2 min, delivered at a flow rate of 3 mL/min. The analysis was based on that originally described by DeGrado and colleagues (17).

Metabolism of D4-FCH and FCH by HCT116 tumor cells. HCT116 cells were grown in T150 flasks in triplicate until they were 70% confluent and then treated with vehicle (1% DMSO in growth medium) or 1 μmol/L PD0325901 in vehicle for 24 h. Cells were pulsed for 1 h with 1.1 MBq D4-FCH or FCH. The cells were washed three times in ice-cold PBS, scraped into 5 mL PBS, and centrifuged at 500 × *g* for 3 min and then resuspended in 2 mL ice-cold methanol for HPLC analysis as described above for tissue samples.

To provide biochemical evidence that the 5′-phosphate was the peak identified on the HPLC chromatogram, cultured cells were treated with alkaline phosphatase as described previously (32). Briefly, HCT116 cells were grown in 100 mm dishes in triplicate and incubated with 5.0 MBq FCH for 60 min at 37°C to form the putative FCH-phosphate. The cells were washed with 5 mL ice-cold PBS twice and then scraped and centrifuged at 750 × *g* (4°C, 3 min) in 5 mL PBS. Cells were homogenized in 1 mL of 5 mmol/L Tris-HCl (pH 7.4) containing 50% (v/v) glycerol, 0.5 mmol/L $MgCl_2$, and 0.5 mmol/L $ZnCl_2$ and incubated with 10 units bacterial (type III) alkaline phosphatase (Sigma) at 37°C in a shaking water bath for 30 min to dephosphorylate the FCH-phosphate. The reaction was terminated by adding ice-cold methanol. Samples were processed as per plasma above and analyzed by radio-HPLC. Control experiments were done without alkaline phosphatase.

Effect of PD0325901 treatment in mice. Size-matched HCT116 tumor-bearing mice were randomized to receive daily treatment by oral gavage of vehicle (0.5% hydroxypropyl methylcellulose + 0.2% Tween 80) or 25 mg/kg (0.005 mL/g mouse) of the mitogenic extracellular kinase inhibitor, PD0325901, prepared in vehicle. D4-FCH-PET scanning was done after 10 daily treatments with the last dose administered 1 h before scanning. After imaging, tumors were snap-frozen in liquid nitrogen and stored at −80°C for analysis of choline kinase A expression.

PET imaging studies. Dynamic FCH and D4-FCH imaging scans were carried out on a dedicated small animal PET scanner, quad-HIDAC (Oxford Positron Systems). The features of this instrument have been described previously (32). For scanning the tail veins, vehicle- or drug-treated mice were cannulated after induction of anesthesia (isofluorane/O_2/N_2O). The animals were placed within a thermostatically controlled jig (calibrated to provide a rectal temperature of ~ 37°C) and positioned prone in the scanner. FCH or D4-FCH (2.96-3.7 MBq) was injected via the tail vein cannula and scanning commenced. Dynamic scans were acquired in list-mode format over a 60 min period as reported previously (33). The acquired data were sorted into 0.5 mm sinogram bins and 19 time frames (0.5 × 0.5 × 0.5 mm voxels; 4 × 15, 4 × 60, and 11 × 300 s) for image reconstruction, which was done by filtered back-projection using a two-dimensional Hamming filter (cutoff 0.6). The image data sets were visualized using the Analyze software (version 6.0; Biomedical Imaging Resource, Mayo Clinic).

Cumulative images of 30 to 60 min dynamic data were used for visualization of radiotracer uptake and to draw regions of interest. Regions of interest were defined manually on five adjacent tumor regions (each 0.5 mm thickness). Dynamic data from these slices were averaged for each tissue (liver, kidney, muscle, urine, and tumor) and at each of the 19 time points to obtain time versus radioactivity curves. Corresponding whole-body time versus radioactivity curves representing injected radioactivity were obtained by adding together radioactivity in all 200 × 160 × 160 reconstructed voxels. Tumor radioactivity was normalized to whole-body radioactivity and expressed as percent injected dose per voxel (%ID/vox). The normalized uptake of radiotracer at 60 min (%ID/vox$_{60}$) was used for subsequent comparisons. The average of the normalized maximum voxel intensity across five slices of tumor %IDvox$_{60max}$ was also use for comparison to account for tumor heterogeneity and existence of necrotic regions in tumor. The area under the curve was calculated as the integral of %ID/vox from 0 to 60 min.

Statistics. Statistical analyses were done using the software GraphPad Prism version 4 (GraphPad). Between-group comparisons were made using the nonparametric Mann-Whitney test. Two-tailed $P \leq 0.05$ was considered significant.

Results

D4-FCH is more resistant to oxidation *in vivo* than FCH. The relative rates of oxidation of the two isotopically radiolabeled choline species, FCH and D4-FCH (see structural formula in Fig. 1*A*), to their respective metabolites, FCH-betaine and D4-FCH-betaine, was evaluated by HPLC in mouse plasma after i.v. injection of the radiotracers; the chromatographic method described previously by DeGrado and colleagues was used (17). As shown in Fig. 1*B*, D4-FCH was markedly more stable to oxidation than FCH with $\sim 40\%$ conversion of D4-FCH to D4-FCH-betaine at 15 min after i.v. injection into mice compared with $\sim 80\%$ conversion of FCH to FCH-betaine. The time course for *in vivo* oxidation is shown in Fig. 1*C*, showing overall improved stability of D4-FCH over FCH. Metabolite analysis of tissues including liver, kidney, and tumor by HPLC was also accomplished. Typical HPLC chromatograms of FCH and D4-FCH and their respective metabolites in tissues are shown in Supplementary Fig. S1. Choline and its metabolites lack any UV chromophore to permit presentation of chromatograms of the cold unlabeled compound simultaneously with the radioactivity chromatograms. Thus, we validated the presence of metabolites by other (chemical and biological) means. Of note, the same chromatographic conditions were used for characterization of the metabolites, and retention times were

Downloaded from http://aacrjournals.org/cancerres/article-pdf/69/19/7721/2614729/7721.pdf by guest on 21 February 2024

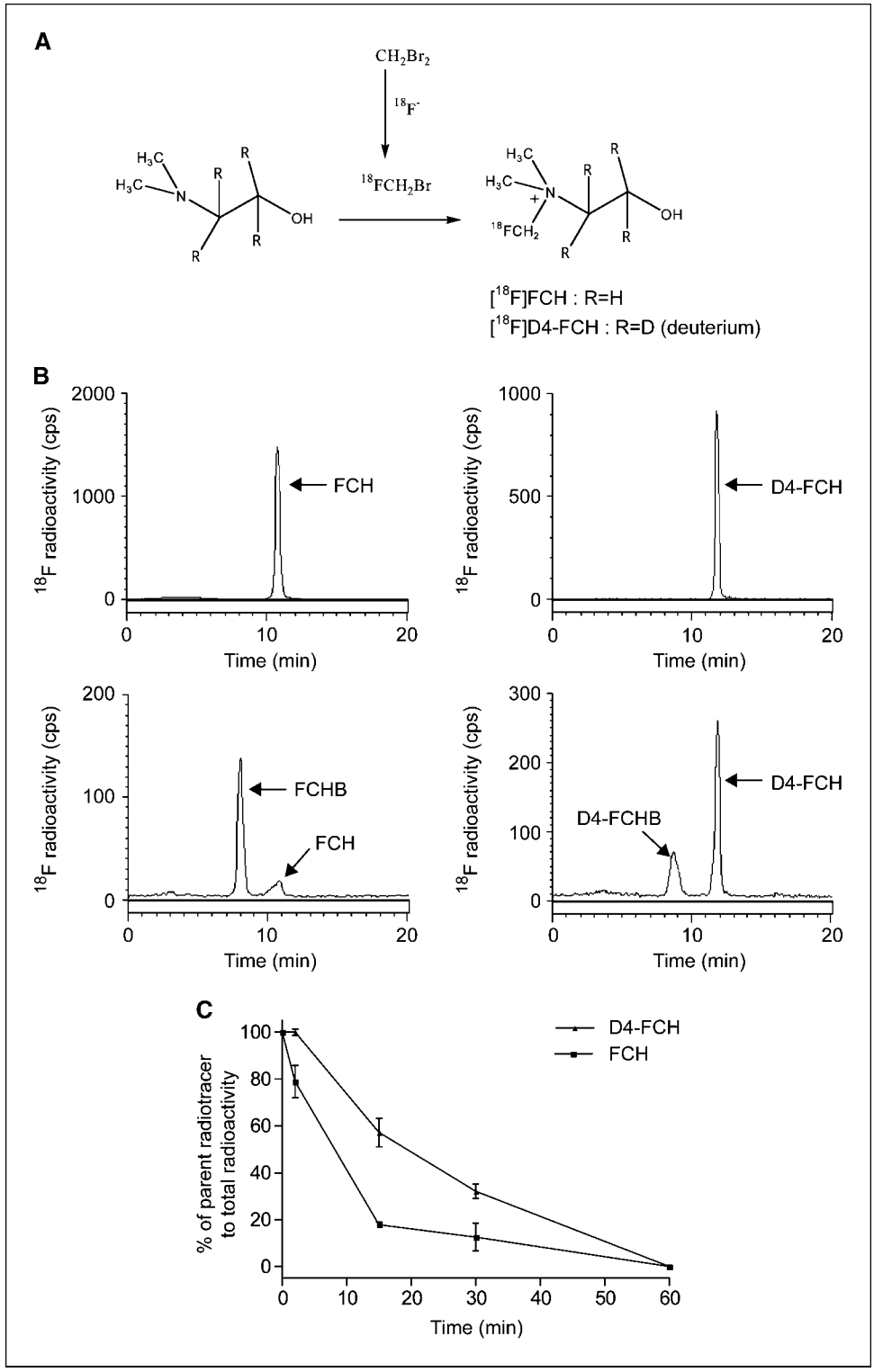

Figure 1. Synthesis of D4-FCH. *A,* no-carrier-added D4-FCH was synthesized by reacting [^{18}F]fluorobromomethane with *N, N*-dimethylaminoethanol or D4-*N*, *N*-dimethylaminoethanol. *B,* analysis of the metabolism of FCH to FCH-betaine and D4-FCH to D4-FCH-betaine by radio-HPLC in mouse plasma samples obtained 15 min after injecting the tracers i.v. into mice. *C,* summary of the conversion of parent tracers, FCH and D4-FCH, to metabolites, FCH-betaine (FCHB) and D4-FCH betaine (D4-FCHB), in plasma. Mean ± SE (n = 3 mice).

similar. We confirmed the identity of the phosphocholine peak biochemically by incubation of the putative phosphocholine formed in untreated HCT116 tumor cells with alkaline phosphatase (Supplementary Fig. S2). Chemical (potassium permanganate) and enzymatic (choline oxidase) methods were used to confirm the identity of the betaine peak (ref. 23; data not shown). A high proportion of liver radioactivity was present as phosphocholine at 30 min post-injection for both FCH and D4-FCH (Fig. 2*A*). An unknown metabolite (possibly the aldehyde intermediate) was observed in both the liver (7.4 ± 2.3%) and the kidney (8.8 ± 0.2%) samples of D4-FCH–treated mice. In contrast, this unknown metabolite was not found in liver samples of FCH-treated mice and only to a smaller extent (3.3 ± 0.6%) in kidney samples. Notably, 60.6 ± 3.7% of D4-FCH–derived kidney radioactivity was

Downloaded from http://aacrjournals.org/cancerres/article-pdf/69/19/7721/2614729/7721.pdf by guest on 21 February 2024

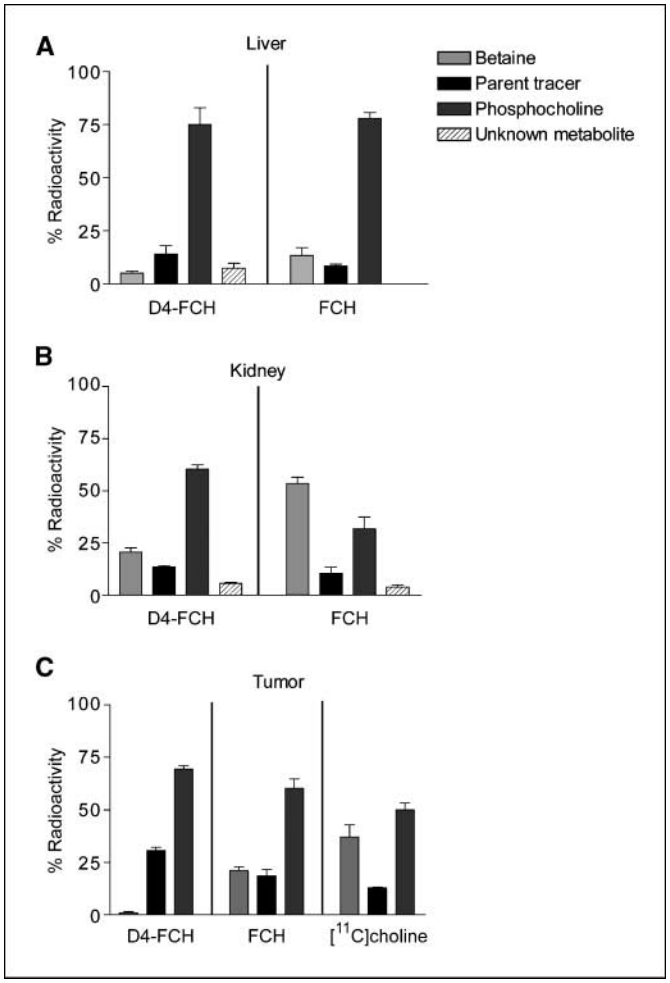

Figure 2. Metabolite profile in mouse tissues after i.v. injection of parent radiotracers, FCH and D4-FCH, assessed by radio-HPLC. The percent radioactivity remaining at 30 min in the form of parent radiotracer, phosphocholine or betaine analogues, as well as that of unknown metabolites is shown for (*A*) liver, (*B*) kidney, and (*C*) HCT116 tumor. In the case of tumor, additional comparisons were done with [^{11}C]choline.

phosphocholine compared with 31.8 ± 9.8% from FCH (P = 0.03). Conversely, most of the FCH-derived radioactivity in the kidney was in the form of FCH-betaine; 53.5 ± 5.3% compared with 20.6 ± 6.2% for D4-FCH (Fig. 2*B*). It could be argued that levels of betaine in plasma reflected levels in tissues such as liver and kidneys. Tumors showed a different HPLC profile compared with liver and kidneys; typical radio-HPLC chromatograms obtained from the analysis of tumor samples (30 min after i.v. injection of FCH, D4-FCH and [^{11}C]choline) are shown in Supplementary Fig. S3. In tumors, radioactivity was mainly in the form of phosphocholine in the case of D4-FCH (Fig. 2*C*). In contrast, both FCH and [^{11}C]choline showed significant levels of FCH-betaine and [^{11}C]betaine. In the context of late imaging, these results indicate that D4-FCH will be the superior radiotracer for PET imaging with an uptake profile that is easier to interpret.

Tissue pharmacokinetics of FCH and D4-FCH by PET. FCH and D4-FCH were both rapidly taken up into tissues and retained (Fig. 3*A* and *B*). Tissue radioactivity increased in the order: muscle < urine < kidney < liver. Given the predominance of phosphorylation over oxidation in the liver (Fig. 2*A*), we found little differences in overall liver radioactivity levels between the two radiotracers. Liver radioactivity at levels 60 min after D4-FCH or FCH injection, %ID/vox$_{60}$, was 20.92 ± 4.24 and 18.75 ± 4.28, respectively (Fig. 3*A* and *B*). This is also in keeping with the lower levels of betaine with D4-FCH injection than with FCH injection (Fig. 2*A*). Thus, pharmacokinetics of the two radiotracers in liver determined by PET (which lacks chemical resolution) were similar. The lower kidney radioactivity levels for D4-FCH compared with FCH (Fig. 3*A* and *B*), on the other hand, reflect the lower oxidation potential of D4-FCH in kidneys (Fig. 2*B*). The %ID/vox$_{60}$ for FCH and D4-FCH were 15.97 ± 4.65 and 7.59 ± 3.91, respectively, in kidneys (Fig. 3*A* and *B*). Urinary excretion was similar between the radiotracers. Regions of interest that were drawn over the bladder showed %ID/vox$_{60}$ values of 5.20 ± 1.71 and 6.70 ± 0.71 for D4-FCH and FCH, respectively. Urinary metabolites comprised mainly the unmetabolized radiotracers (data not shown). Muscle showed the lowest radiotracer levels of any tissue.

D4-FCH shows higher sensitivity for imaging tumors by PET. Given the relatively high systemic stability of D4-FCH and high proportion of phosphocholine metabolites, it was reassuring to observe higher tumor radiotracer uptake by PET in mice that were injected with D4-FCH compared with the FCH group.

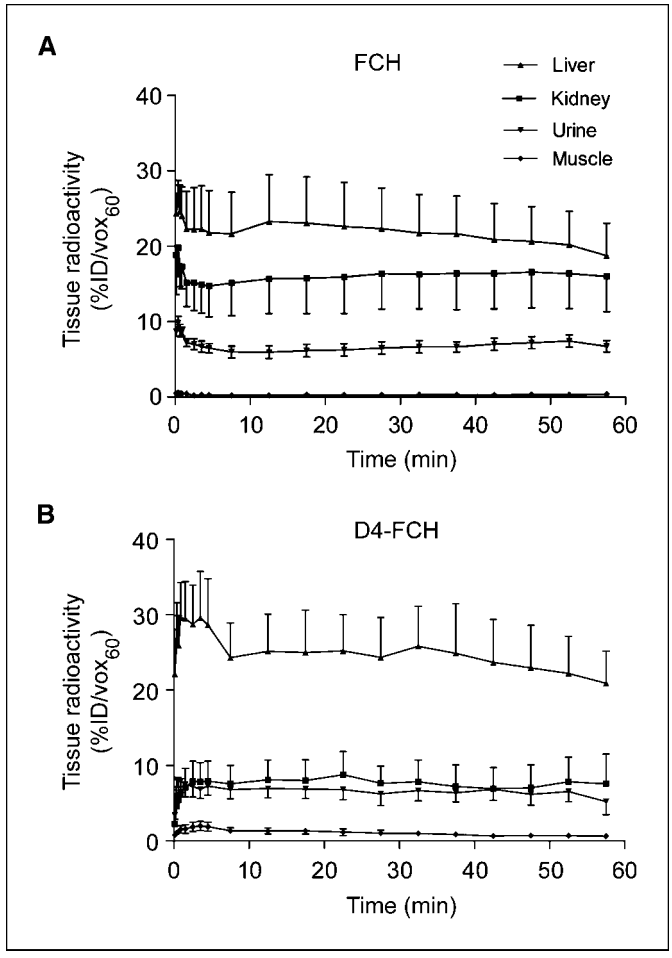

Figure 3. Tissue profile of FCH and D4-FCH. *A,* time versus radioactivity curve for the uptake of FCH in liver, kidney, urine (bladder), and muscle, derived from PET data. *B,* corresponding data for D4-FCH. Mean ± SE (n = 4 mice). For clarity, top and bottom error bars (SE) have been used.

Downloaded from http://aacrjournals.org/cancerres/article-pdf/69/19/7721/2614729/7721.pdf by guest on 21 February 2024

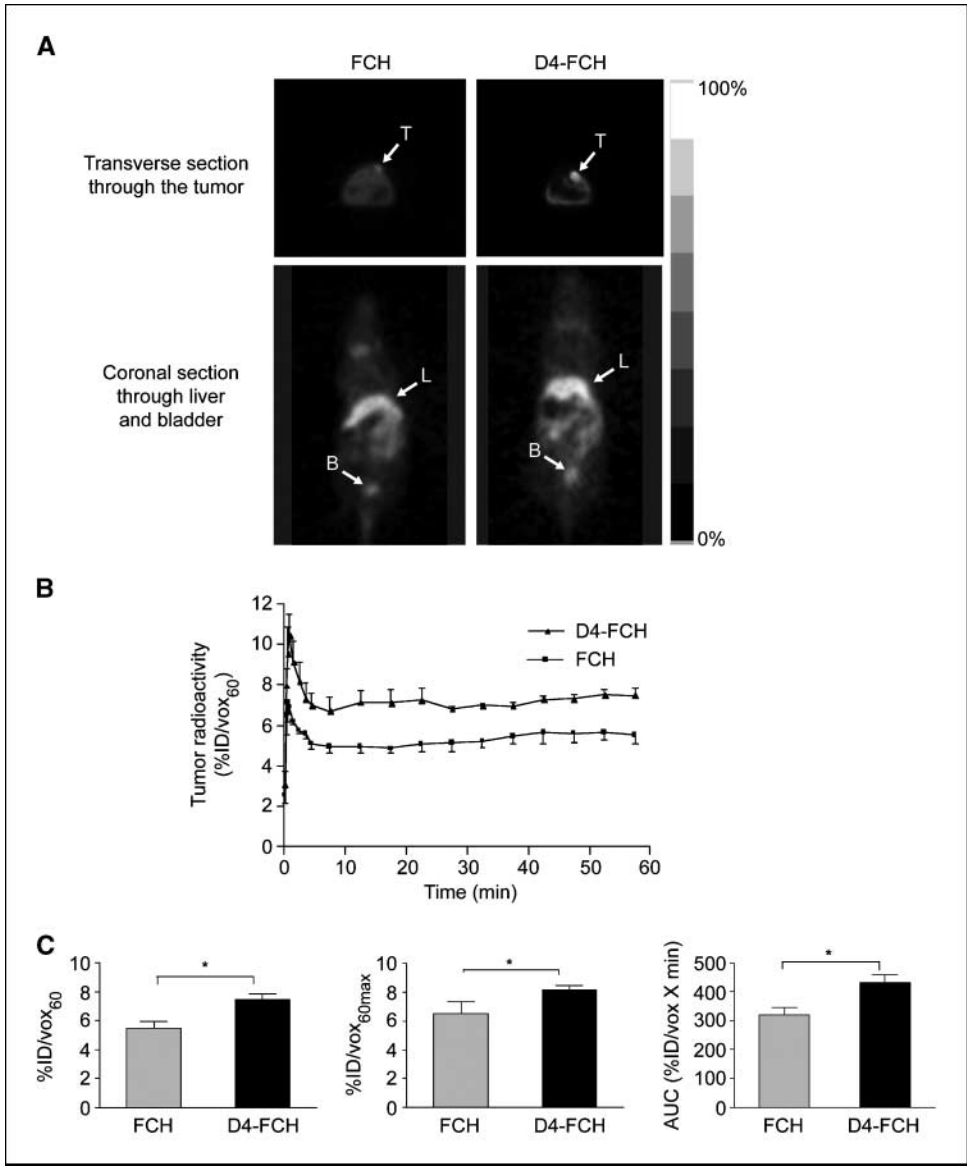

Figure 4. Tumor profile of FCH and D4-FCH in SKMEL-28 tumor xenograft. *A,* typical FCH-PET and D4-FCH-PET images of SKMEL-28 tumor-bearing mice showing 0.5 mm transverse sections through the tumor and coronal sections through the bladder. For visualization, 30 to 60 min summed image data are displayed. *Arrows,* tumors (*T*), liver (*L*), and bladder (*B*). *B,* comparison of time versus radioactivity curves for FCH and D4-FCH in tumors. For each tumor, radioactivity at each of 19 time frames was determined. Mean ± SE %ID/vox$_{60}$ (n = 4 mice per group). *C,* summary of imaging variables. Mean ± SE (n = 4). *, P = 0.04. For clarity, top and bottom error bars (SE) have been used.

Figure 4*A* shows typical (0.5 mm) transverse PET image slices showing accumulation of FCH and D4-FCH in human melanoma SKMEL-28 xenografts. In this mouse model, the tumor signal-to-background contrast was qualitatively superior in the D4-FCH PET images compared with FCH images. Both radiotracers had similar tumor kinetic profiles detected by PET (Fig. 4*B*). The kinetics were characterized by rapid tumor influx with peak radioactivity at ~1 min (Fig. 4*B*). Tumor levels then equilibrated until ~5 min followed by a plateau. The delivery and retention of D4-FCH were quantitatively higher than those for FCH (Fig. 4*C*). The %ID/vox$_{60}$ for D4-FCH and FCH were 7.43 ± 0.47 and 5.50 ± 0.49, respectively (P = 0.04). Because tumors often present with heterogeneous population of cells, we exploited another imaging variable that is probably less sensitive to experimental noise, an average of the maximum pixel %ID/vox$_{60}$ across five slices (%IDvox$_{60max}$). This variable was also significantly higher for D4-FCH (P = 0.05; Fig. 4*C*). Furthermore, tumor area under the time versus radioactivity curve was higher for D4-FCH mice than FCH (P = 0.02). Although the 30 min time point was selected for a more detailed analysis of tissue samples, it should be noted that the percentage of parent compound in plasma was consistently higher for D4-FCH compared with FCH at earlier time points. Regarding imaging, tumor uptake for both radiotracers was similar at the early (15 min) and late (60 min) time points (Supplementary Table S1). The earlier time points may be appropriate for pelvic imaging.

D4-FCH detects response to treatment. Having shown that D4-FCH was a more stable fluorinated-choline analogue for *in vivo* studies, we wanted to investigate if this radiotracer could be used to measure response to therapy. We chose to perform these studies in a reproducible tumor model system in which treatment outcomes have been previously characterized, that is, the human colon carcinoma xenograft HCT116 treated with PD0325901 daily for 10 days (31). Drug treatment led to tumor stasis (reduction in tumor size by only 12.2% at day 10 compared with the pretreatment group); tumors of vehicle-treated mice increased by 375%. Tumor D4-FCH levels in PD0325901-treated mice peaked at approximately the same time as those of vehicle-treated ones; however, there

Downloaded from http://aacrjournals.org/cancerres/article-pdf/69/19/7721/2614729/7721.pdf by guest on 21 February 2024

was a marked reduction in radiotracer retention in the treated tumors (Fig. 5*A*). All imaging variables decreased after 10 days of drug treatment ($P = 0.05$, Fig. 5*B*). This indicates that D4-FCH can be used to detect treatment response even under conditions where large changes in tumor size reduction are not seen (31). To understand the biomarker changes, we examined the intrinsic cellular effect of PD0325901 on D4-FCH-phosphocholine formation by treating exponentially growing HCT116 cells in culture with PD0325901 for 24 h and measuring the 60 min uptake of D4-FCH *in vitro*. As shown in Fig. 5*C*, PD0325901 significantly inhibited D4-FCH-phosphocholine formation in drug-treated cells, showing that the effect of the drug in tumors is likely due to cellular effects on choline metabolism rather than hemodynamic effects.

To understand further the mechanisms regulating D4-FCH uptake with drug treatment, we assessed changes in choline kinase A expression in PD0325901- and vehicle-treated tumors excised after PET scanning. A significant reduction in choline kinase A protein expression was seen *in vivo* at day 10 ($P = 0.03$) following PD0325901 treatment (Fig. 6), indicating that reduced choline kinase A expression contributed to the lower D4-FCH uptake in drug-treated tumors. The drug-induced reduction of choline kinase A expression also occurred *in vitro* in exponentially growing cells treated with PD0325901 (data not shown).

Discussion

We have designed, synthesized, and established utility of a novel radiolabeled choline analogue for tumor imaging. Many cancers have elevated phospholipid biosynthesis to meet the demand of rapid tumor cell growth, and in these cancers, phosphocholine serves as an important mediator of transmembrane signaling (34, 35). Choline is taken into cells by a specific transport mechanism and phosphorylated by choline kinase, which is constitutively active in many cancer cells (10, 36, 37). This metabolic process serves to trap choline in cells as phosphocholine; thus, radiolabeled analogues of choline are being explored as radiotracers for imaging tumors by PET. FCH, originally developed by DeGrado and colleagues, is currently being evaluated for imaging prostate cancer and other malignancies (17, 22, 38, 39). In this study, we report the development of a more stable FCH analogue, D4-FCH, for cancer detection in which substitution of deuterium for hydrogen on the ethyl alcohol portion of choline results in a large observed isotope effect in the oxidation of choline to betaine by choline oxidase (25–27). Kinetic studies indicate that the magnitude of the $^{1}H/^{2}D$ isotope effect is the result of environmentally enhanced quantum tunneling involving a highly preorganized enzyme active site, where the probability of tunneling decreases with the increased mass of deuterium in a molecule

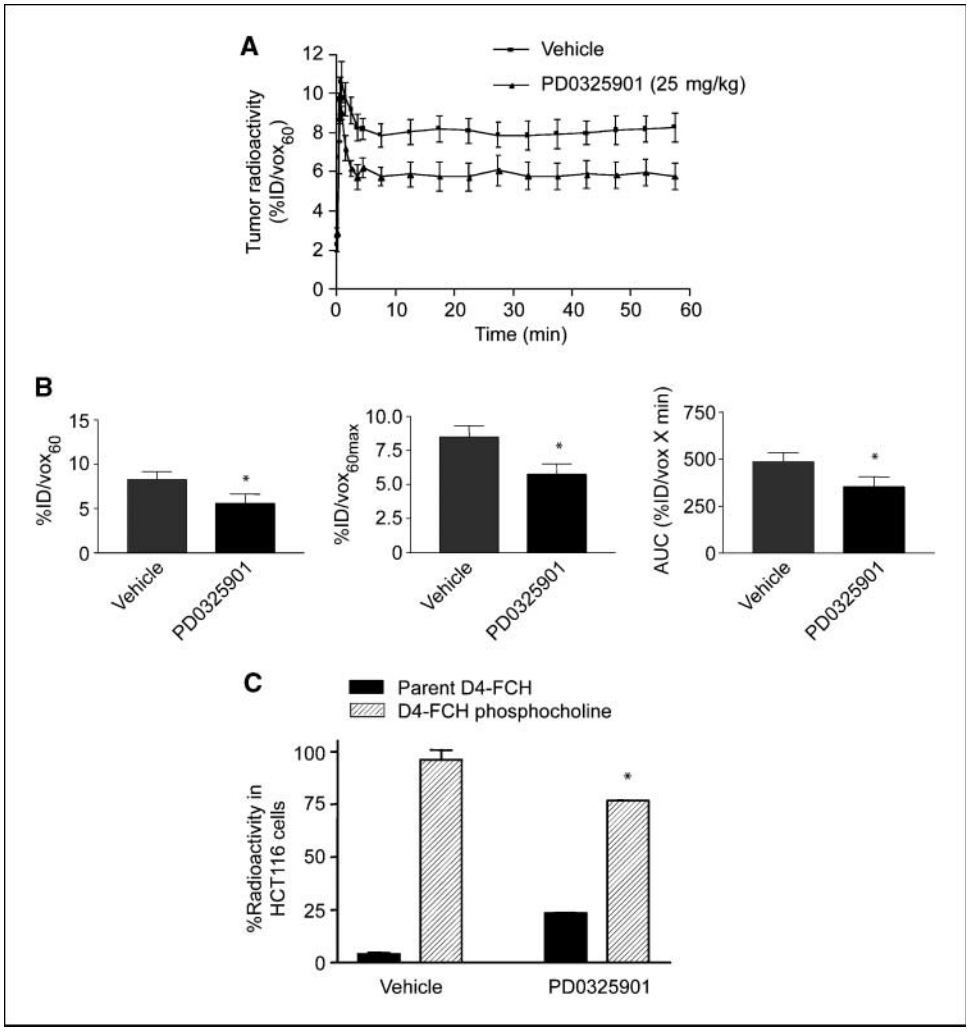

Figure 5. Effect of PD0325901 on uptake of D4-FCH in HCT116 tumors and cells. *A,* normalized time versus radioactivity curves in HCT116 tumors following daily treatment for 10 d with vehicle or 25 mg/kg PD0325901. Mean ± SE ($n = 3$ mice). *B,* summary of imaging variables $\%ID/vox_{60}$, $\%ID/vox_{60max}$, and area under the curve. Mean ± SE. *, $P = 0.05$. *C,* intrinsic cellular effect of PD0325901 (1 μmol/L) on D4-FCH phosphocholine metabolism after treating HCT116 cells for 1 h with D4-FCH in culture. Mean ± SE ($n = 3$). *, $P = 0.03$.

Downloaded from http://aacrjournals.org/cancerres/article-pdf/69/19/7721/2614729/7721.pdf by guest on 21 February 2024

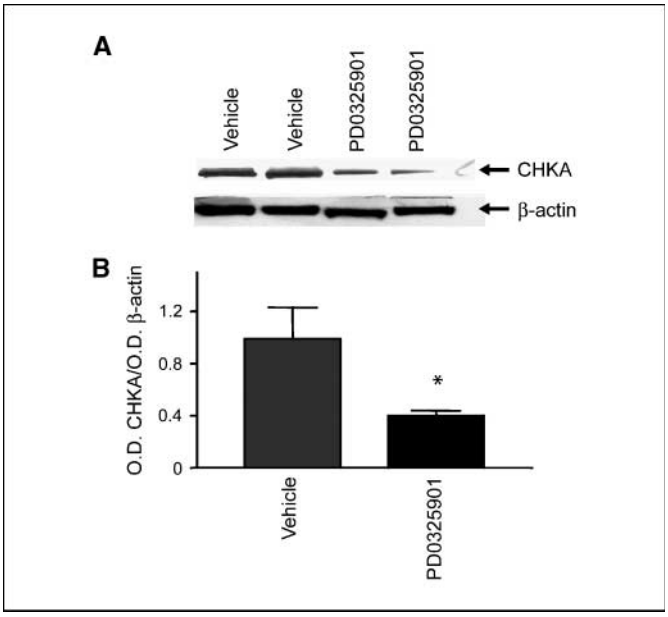

Figure 6. Expression of choline kinase A in HCT116 tumors. *A,* typical Western blot showing the effect of PD0325901 on tumor choline kinase A (*CHKA*) protein expression. HCT116 tumors from mice that were injected with PD0325901 (25 mg/kg/d for 10 d, orally) or vehicle were analyzed for choline kinase A expression by Western blotting. β-Actin was used as the loading control. *B,* summary densitometer measurements for choline kinase A expression expressed as a ratio to β-actin. Mean ± SE ratios ($n = 3$). *, $P = 0.05$. *O.D.,* absorbance.

(24). The biological effect of this substitution is to reduce oxidation and increase the net availability of the parent tracer for phosphorylation and trapping within cells leading to improved signal-to-background contrast for PET imaging of tumors *in vivo* (40–42).

Improved stability of D4-FCH over FCH for late imaging after clearance was supported initially (0-30 min) by the higher proportion of parent radiotracer in plasma, but this difference appeared to have been lost by 60 min when the parent radiotracers had been completely metabolized (Fig. 1*C*). We interpret this finding as a model limitation: the capacity of rodents to metabolize choline analogues (43) is substantially higher than that of humans (23), so we expect the early differential between the two radiotracers to be maintained in humans. Improved stability of D4-FCH over FCH was shown as reduced levels of D4-FCH oxidation products in plasma of mice injected i.v. with the radiotracers. The oxidation product of D4-FCH was also lower in at least one of two major organs responsible for choline oxidation/choline oxidase activity, the liver and the kidney (23, 39, 43). The reduced oxidation of D4-FCH resulted, for instance, in a 2-fold lower total radioactivity level in kidney. Tissue HPLC analysis also confirmed that most of the D4-FCH was trapped specifically in the form of phosphocholine, whereas betaine was the main metabolite from FCH in kidneys. It is possible that kidneys have a lower capacity for phosphorylating the free D4-FCH. In liver, on the other hand, unmetabolized FCH and D4-FCH were rapidly phosphorylated and the predominance of phosphorylation may explain the similar levels of liver radioactivity for both radiotracers. Notably, betaine levels in liver were higher for FCH than D4-FCH. Betaine, like phosphocholine, is a charged molecule and is also expected to be trapped in cells to a reasonable extent; unlike phosphocholine, however, it is exported into circulation as shown in this study.

One advantage of using radiolabeled choline analogues for pelvic imaging is their low renal elimination. Urine levels of choline analogues result largely from unmetabolized parent radiotracer (data not shown), as betaine analogues are efficiently reabsorbed in the kidney tubules (44, 45). Due to their ionization properties, oxidation intermediates (such as aldehyde) are unlikely to be reabsorbed efficiently within the kidney tubules and could contribute to urinary radioactivity (45). It was a concern that the high stability of D4-FCH, and hence higher levels of parent radiotracer in plasma, will lead to high levels of radioactivity in the urine. Compared to [^{11}C]choline, FCH was found to have less desirable urinary excretion properties. We have not been able to show that D4-FCH used under the same conditions will overcome this limitation. It may be possible, however, for patients to void urine at late time points to reduce bladder radioactivity.

Of interest, both FCH and [^{11}C]choline showed high levels of betaine metabolites in tumor, whereas very little betaine metabolite was found following D4-FCH injection. The improved stability of D4-FCH will permit late imaging to be performed with confidence because metabolism will be less of a concern. In a late imaging protocol, voiding can further reduce the spillover contribution of bladder radioactivity. Improved stability of D4-FCH also led to increased tumor radioactivity by 1.3-fold compared with FCH. This increased tumor retention could be ascribed to increased availability of substrate for phosphorylation and reduced competing (oxidation) reactions that leads to betaine formation and elimination of the latter. Having shown superior pharmacokinetics, we further established utility of D4-FCH for response monitoring. D4-FCH was found to be a useful radiotracer for monitoring the effect of MEK inhibition by PD0325901 in a model where the drug effects are largely cytostatic at the dose used. The reduction in radiotracer uptake following drug treatment *in vivo* was intrinsic to changes in cellular biochemistry as shown *in vitro* and could be ascribed at least in part to reduced choline kinase A expression.

In translating our findings into clinical imaging, it should be noted that oxidation of choline is faster in rodents (38) compared with humans (23). Thus, we expect the rate of D4-FCH oxidation to be even lower in humans; this may lead to further improvements in detection sensitivity in humans consequent to the higher overall levels of phosphorylated D4-FCH. In conclusion, we have shown that the novel radiotracer, D4-FCH, has improved stability and sensitivity for detection of choline metabolism *in vivo*. The radiotracer also has potential for detecting response to anticancer drug treatment. These promising attributes warrant further preclinical and clinical development of D4-FCH.

Disclosure of Potential Conflicts of Interest

No potential conflicts of interest were disclosed.

Acknowledgments

Received 4/16/09; revised 6/16/09; accepted 7/23/09; published OnlineFirst 9/22/09.

Grant support: Cancer Research UK and Engineering and Physical Sciences Research Council (C2536/A10337), and UK Medical Research Council (U1200.005.00001.01).

The costs of publication of this article were defrayed in part by the payment of page charges. This article must therefore be hereby marked *advertisement* in accordance with 18 U.S.C. Section 1734 solely to indicate this fact.

Downloaded from http://aacrjournals.org/cancerres/article-pdf/69/19/7721/2614729/7721.pdf by guest on 21 February 2024

References

1. Aboagye EO, Bhujwalla ZM. Malignant transformation alters membrane choline phospholipids metabolism of human mammary epithelial cell. Cancer Res 1999;59:80–4.
2. Exton JH. Phosphatidylcholine breakdown and signal transduction. Biochim Biophys Acta 1994;1212:26–42.
3. George TP, Morash SC, Cook HW, Byers DM, Palmer FBSC, Spence MW. Phosphatidylcholine biosynthesis in cultured glioma cells: evidence for channelling of intermediates. Biochim Biophys Acta 1989;104:283–91.
4. Teegarden D, Taparowsky EJ, Kent C. Altered phosphatidylcholine metabolism in C3H10T1/2 cells transfected with the Harvey-ras oncogene. J Biol Chem 1990; 265:6042–7.
5. Aoyama C, Liao H, Ishidate K. Structure and function of choline kinase isoforms in mammalian cells. Prog Lipid Res 2004;43:266–81.
6. Glunde K, Jie C, Bhujwalla ZM. Molecular causes of the aberrant choline phospholipid metabolism in breast cancer. Cancer Res 2004;64:4270–6.
7. Glunde K, Raman V, Mori N, Bhujwalla ZM. RNA interference-mediated choline kinase suppression in breast cancer cells induces differentiation and reduces proliferation. Cancer Res 2005;65:11034–43.
8. Iorio E, Mezzanzanica D, Alberti P, et al. Alterations of choline phospholipid metabolism in ovarian tumor progression. Cancer Res 2005;65:9369–76.
9. Ramirez de Molina A, Rodriguez-Gonzalez A, Gutierrez R, et al. Overexpression of choline kinase is a frequent feature in human tumor-derived cell lines and in lung, prostate, and colorectal human cancers. Biochem Biophys Res Commun 2002;296:580–3.
10. Ramirez de Molina A, Sarmentero-Estrada J, Belda-Iniesta C, et al. Expression of choline kinase α to predict outcome in patients with early-stage non-small-cell lung cancer: a retrospective study. Lancet Oncol 2007;8:889–97.
11. Hara T, Inagaki K, Kosaka N, Morita T. Sensitive detection of mediastinal lymphnode metastasis of lung cancer with [^{11}C]-choline PET. J Nucl Med 2000; 41:1507–13.
12. Hara T, Kosaka N, Kishi H. PET imaging of prostate cancer using carbon-11-choline. J Nucl Med 1998;39: 990–5.
13. Hara T, Kosaka N, Shinoura N, Kondo T. PET imaging of brain tumor with [methyl-^{11}C]choline. J Nucl Med 1997;38:842–7.
14. Kobori O, Kirihara Y, Kosaka N, Hara T. Positron emission tomography of esophageal carcinoma using [^{11}C]-choline and ^{18}F-fluorodeoxyglucose. Cancer Cell 1999;86:1638–48.
15. Pieterman RM, Que TH, Elsinga PH, et al. Comparison of [^{11}C]-choline and [^{18}F]-FDG PET in primary diagnosis and staging of patients with thoracic cancer. J Nucl Med 2002;43:167–72.
16. Reske SN. ^{11}C-Choline uptake with PET/CT for the initial diagnosis of prostate cancer: relation to PSA levels, tumour stage and anti-androgenic therapy. Eur J Nucl Med Mol Imaging 2008;35:1741.
17. DeGrado TR, Coleman RE, Wang S, et al. Synthesis and evaluation of [^{18}F]-labeled choline as an oncologic tracer for positron emission tomography: initial findings in prostate cancer. Cancer Res 2001;61:110–7.
18. Beheshti M, Vali R, Waldenberger P, et al. Detection of bone metastases in patients with prostate cancer by ^{18}F fluorocholine and [^{18}F]-fluoride PET-CT: a comparative study. Eur J Nucl Med Mol Imaging 2008;35: 1766–74.
19. Cimitan M, Bortolus R, Morassut S, et al. [^{18}F]-fluorocholine PET/CT imaging for the detection of recurrent prostate cancer at PSA relapse: experience in 100 consecutive patients. Eur J Nucl Med Mol Imaging 2006;33:1387–98.
20. de Jong IJ, Pruim J, Elsinga PH, Jongen MM, Mensink HJ. Vaalburg W. Visualization of bladder cancer using ^{11}Ccholine PET: first clinical experience. Eur J Nucl Med Mol Imaging 2002;29:1283–8.
21. Price DT, Coleman RE, Liao RP, Robertson CN, Polascik TJ, DeGrado TR. Comparison of [^{18}F]fluorocholine and [^{18}F]fluorodeoxyglucose for positron emission tomography of androgen dependent and androgen independent prostate cancer. J Urol 2002;168:273–80.
22. DeGrado TR, Reiman RE, Price DT, Wang S, Coleman RE. Pharmacokinetics and radiation dosimetry of [^{18}F]-fluorocholine. J Nucl Med 2002;43:92–6.
23. Roivainen A, Forsback S, Gronroos T, et al. Blood metabolism of [methyl-^{11}C]choline; implications for *in vivo* imaging with positron emission tomography. Eur J Nucl Med 2000;27:25–32.
24. Fan F, Gadda G. An internal equilibrium preorganizes the enzyme-substrate complex for hydride tunneling in choline oxidase. Biochemistry 2007;46:6402–8.
25. Fan F, Gadda G. On the catalytic mechanism of choline oxidase. J Am Chem Soc 2005;127:2067–74.
26. Gadda G. pH and deuterium kinetic isotope effects studies on the oxidation of choline to betaine-aldehyde catalyzed by choline oxidase. Biochim Biophys Acta 2003;1650:4–9.
27. Nagel ZD, Klinmn JP. Tunneling and dynamics in enzymatic hydride transfer. Chem Rev 2006;106: 3095–118.
28. Bergman J, Eskola O, Lehikoinen P, Solin O. Automated synthesis and purification of [^{18}F]bromofluoromethane at high specific radioactivity. Appl Radiat Isot 2001;54:927–33.
29. Pascali C, Itawa R, Cambiè M, Bombardieri E. [^{11}C]-Methylation on a C18 Sep-Pak cartridge: a convenient way to produce [*N*-methyl-^{11}C]choline. J Labelled Compds Radiopharm 2000;43:195–203.
30. Workman P, Balmain A, Hickman JA, et al. UKCCCR guidelines for the welfare of animals in experimental neoplasia. Lab Anim 1988;22:195–201.
31. Leyton J, Smith G, Lees M, et al. Noninvasive imaging of cell proliferation following mitogenic extracellular kinase inhibition by PD0325901. Mol Cancer Ther 2008; 7:3112–21.
32. Barthel H, Cleij MC, Collingridge DR, et al. 3′-Deoxy-3′-[^{18}F]fluorothymidine as a new marker for monitoring tumor response to antiproliferative therapy *in vivo* with positron emission tomography. Cancer Res 2003;63: 3791–8.
33. Leyton J, Alao JP, Da Costa M, et al. *In vivo* biological activity of the histone deacetylase inhibitor LAQ824 is detectable with 3′-deoxy-3′-[^{18}F]fluorothymidine positron emission tomography. Cancer Res 2006;66:7621–9.
34. Zeisel SH. Choline phospholipids: signal transduction and carcinogenesis. FASEB J 1993;7:551–7.
35. Zeisel SH. Nutrients, signal transduction and carcinogenesis. Adv Exp Med Biol 1995;369:175–83.
36. Katz-Brull R, Degani H. Kinetics of choline transport and phosphorylation in human breast cancer cells; NMR application of the zero trans method. Anticancer Res 1996;16:1375–80.
37. Katz-Brull R, Seger D, Rivenson-Segal D, Rushkin E, Degani H. Metabolic markers of breast cancer: enhanced choline metabolism and reduced choline-ether-phospholipid synthesis. Cancer Res 2002;62:1966–70.
38. Bensal A, Shuyan W, Hara T, Harris RA, Timothy R, DeGrado TR. Biodisposition and metabolism of [^{18}F]fluorocholine in 9L glioma cells and 9L glioma-bearing Fisher rats. Eur J Nucl Med Mol Imaging 2008;35: 1192–203.
39. Kwee SA, DeGrado TR, Talbot JN, Gutman F, Coel MN. Cancer imaging with fluorine-18-labeled choline derivatives. Semin Nucl Med 2007;37:420–8.
40. Fowler JS, Wolf AP, MacGregor RR, et al. Mechanistic positron emission tomography studies: demonstration of a deuterium isotope effect in the monoamine oxidase-catalyzed binding of [^{11}C]L-deprenyl in living baboon brain. J Neurochem 1988;51:1524–34.
41. Schou M, Halldin C, Sovago J, et al. PET evaluation of novel radiofluorinated reboxetine analogs as norepinephrine transporter probes in the monkey brain. Synapse 2004;53:57–67.
42. van Dyck CH, Soares JC, Tan PZ, et al. Equilibrium modeling of 5-HT(2A) receptors with [^{18}F]-deuteroaltanserin and PET: feasibility of a constant infusion paradigm. Nucl Med Biol 2000;27:715–22.
43. Haubrich DR, Wang PF, Wedeking PW. Distribution and metabolism of intravenously administered choline[methyl-3-H] and synthesis *in vivo* of acetylcholine in various tissues of guinea pigs. J Pharmacol 1975;193: 246–55.
44. Lever M, Sizeland PC, Bason LM, Hayman CM, Chambers ST. Glycine betaine and proline betaine in human blood and urine. Biochim Biophys Acta 1994; 1200:259–64.
45. Pummer S, Dantzler WH, Lien YH, Moeckel GW, Volker K, Silbernagl S. Reabsorption of betaine in Henle's loops of rat kidney *in vivo*. Am J Physiol Renal Physiol 2000;278:F434–9.

Downloaded from http://aacrjournals.org/cancerres/article-pdf/69/19/7721/2614729/7721.pdf by guest on 21 February 2024